PHYSICAL REVIEW B **92**, 140303(R) (2015)

Strong anharmonicity induces quantum melting of charge density wave in $2H$-$NbSe_2$ under pressure

Maxime Leroux,[1,*] Ion Errea,[2,3,4] Mathieu Le Tacon,[5] Sofia-Michaela Souliou,[5] Gaston Garbarino,[6] Laurent Cario,[7] Alexey Bosak,[6] Francesco Mauri,[4] Matteo Calandra,[4,†] and Pierre Rodière[1,‡]

[1]*Université Grenoble Alpes, CNRS, I. Néel, F-38000 Grenoble, France*

[2]*Donostia International Physics Center (DIPC), Manuel de Lardizabal Pasealekua 4, 20018 Donostia-San Sebastián, Basque Country, Spain*

[3]*IKERBASQUE, Basque Foundation for Science, 48011 Bilbao, Spain*

[4]*IMPMC, UMR CNRS 7590, Sorbonne Universités–UPMC Univ. Paris 06, MNHN, IRD, 4 Place Jussieu, F-75005 Paris, France*

[5]*Max-Planck-Institut für Festkörperforschung, Heisenbergstrße 1, D-70569 Stuttgart, Germany*

[6]*European Synchrotron Radiation Facility, Grenoble, France*

[7]*Institut des Matériaux Jean Rouxel (IMN), Université de Nantes, CNRS, 2 rue de la Houssinière, Boîte Postale 3229, 44322 Nantes, France*

(Received 17 June 2015; published 21 October 2015)

The pressure and temperature dependence of the phonon dispersion of $2H$-$NbSe_2$ is measured by inelastic x-ray scattering. A strong temperature dependent soft phonon mode, reminiscent of the charge density wave (CDW), is found to persist up to a pressure as high as 16 GPa, far above the critical pressure at which the CDW disappears at 0 K. By using *ab initio* calculations beyond the harmonic approximation, we obtain an accurate, quantitative description of the (P,T) dependence of the phonon spectrum. Our results show that the rapid destruction of the CDW under pressure is related to the zero mode vibrations—or quantum fluctuations—of the lattice renormalized by the anharmonic part of the lattice potential. The calculations also show that the low-energy longitudinal acoustic mode that drives the CDW transition barely contributes to superconductivity, explaining the insensitivity of the superconducting critical temperature to the CDW transition.

DOI: 10.1103/PhysRevB.92.140303 PACS number(s): 71.45.Lr, 74.70.Ad, 74.62.Fj, 74.25.Kc

The interplay between charge density wave order, i.e., a static modulation of the electronic density close to the Fermi level, and superconductivity has attracted much attention [1,2]. This is the central issue of a long-standing debate in simple transition-metal dichalcogenides without strong electronic correlations, such as $2H$-$NbSe_2$ [3,4]. At $T_{CDW} = 33.5$ K, $2H$-$NbSe_2$ undergoes a second order phase transition towards an incommensurate CDW phase which coexists with superconductivity below $T_c = 7.2$ K. The anisotropy and temperature dependence of the electronic band structure has been widely studied by ARPES and STM measurements [5–11]. The CDW is coupled to a periodic lattice distortion through a strong electron-phonon coupling. The transition is associated with a softening of a longitudinal acoustic phonon mode as temperature is lowered to T_{CDW} [12]. It was already noticed that the high order phonon fluctuations and strong electron-phonon interactions explain some of the key features of the formation of the CDW in this system [13,14]. In the specific case of $NbSe_2$ at ambient pressure, the reduction of the phonon lifetime through the electron-phonon coupling is a key ingredient in the temperature dependence of the phonon dispersion [15].

At ambient pressure, published *ab initio* calculations successfully reproduce the lattice instability on a wide part of the Brillouin zone around the experimentally observed $\mathbf{q}_{\mathrm{CDW}}$ [12,16,17]. However, these calculations are carried out at the harmonic level, and therefore at $T = 0$ K. The temperature dependence can be qualitatively reproduced using a Gaussian smearing of the Fermi surface which reduces the contribution of the electron-phonon interaction. Quantitatively however, the temperatures that would effectively yield this smearing are unphysical, as they exceed the experimentally observed one by several orders of magnitude.

The quantitative failure of the harmonic *ab initio* calculations is even worse under pressure. Experimentally, by applying a hydrostatic pressure, T_{CDW} is driven to 0 K and the CDW instability disappears above the critical pressure P_{CDW} $(T = 3.5\ \mathrm{K}) = 4.6$ GPa [18]. Around this quantum phase transition superconductivity remains essentially unaffected, as shown on the (T,P) phase diagram in Fig. 1 [19,20]. However, harmonic *ab initio* calculations fail to describe the ground state of $NbSe_2$ as a function of pressure [see Supplemental Material (SM) [21] and [22]]. Indeed, they predict (see Fig. 3 and SM) a CDW instability up to $P_C = 14$ GPa, a pressure that largely exceeds the experimentally observed one. This persistence of the CDW instability in the harmonic calculations is reminiscent of the effect of isovalent and isoelectronic substitution of Se with lighter S. The harmonic calculation also predicts a CDW instability for NbS_2 that is not observed experimentally [23].

Taken together, these facts indicate that for an accurate description of the ground state (even at $T = 0$ K) of these systems, calculations beyond the standard harmonic approximation must be carried out. The impact of anharmonicity has recently been highlighted in different systems. To mention only a few, the thermodynamical properties of the metal-insulator transition in strongly correlated VO_2 [24], the transport properties of thermoelectric PbTe [25], or the electron-phonon interaction above the Verwey transition in magnetite Fe_3O_4 [26] are all strongly influenced by anharmonicity. Even at low temperatures, where its effects are expected to be weaker, it must be taken into account to explain the pressure dependence of the crystal structure of calcium [27], the inverse isotope

*Present address: Materials Science Division, Argonne National Laboratory, 9700 S. Cass Avenue, Argonne, Illinois 60439, USA; mleroux@anl.gov

†matteo.calandra@upmc.fr

‡pierre.rodiere@neel.cnrs.fr

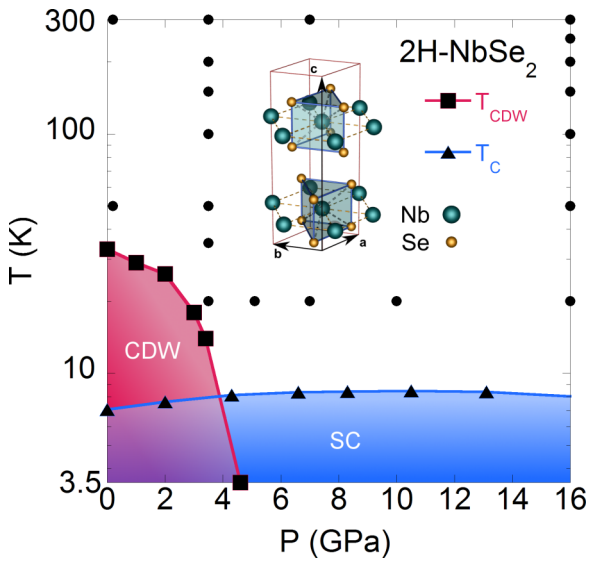

FIG. 1. (Color online) Phase diagram of $NbSe_2$. Squares indicate the limit of the CDW phase measured in Ref. [19] with the addition of the point at 4.6 GPa from Ref. [18], triangles indicate the superconducting T_c measured in [20], and circles indicate the pressure and temperature of our IXS measurements. Inset: crystallographic structure of $2H$-$NbSe_2$ [3].

effect in superconducting PdH [28], or the phonon spectra at the proximity of the liquid-solid transition of helium at 0 K [29]. Finally, anharmonicity is crucial for understanding the ground state of a system when a quantum electronic phase transition coupled to the lattice occurs, as in, e.g., ferroelectrics [30] or CDW compounds [12,14,23,31]. In most cases, however, these effects are computationally too expensive to be evaluated in standard first-principle calculations, and therefore often disregarded.

Here, we report the investigation of the temperature and pressure dependence of the phonon spectra of $NbSe_2$ by using high resolution inelastic x-ray scattering (IXS) from a crystal in a diamond anvil cell, up to pressures as large as 16 GPa at $T = 20$ K. We observe that the strong temperature dependence of the soft phonon mode is reduced by pressure, but still present even at 16 GPa.

We show that the temperature and pressure dependence of the phonon spectra can be accurately accounted for when the effects of anharmonicity are explicitly included in the calculation. Anharmonic effects were calculated within the newly developed stochastic self-consistent harmonic approximation (SSCHA), yielding an unprecedented agreement with the experimentally determined temperature dependence of the phonon spectra at various pressures. We show that at low temperatures, for pressures between P_{CDW} and P_C, the CDW is destroyed by quantum fluctuations, which easily overcome the double-well lattice potential and, thus, are strongly affected by the anharmonic part of the potential. Surprisingly, we observe that anharmonic effects dominate the low-energy phonon spectrum of $2H$-$NbSe_2$ in a large pressure range, extending at least up to 16 GPa $\gg P_{CDW}$ and down to the lowest temperatures. Finally, we demonstrate that a large electron-phonon interaction, mostly due to optical modes rather than to the soft longitudinal acoustic mode which drives the CDW instability, contributes substantially to superconductivity in $2H$-$NbSe_2$, and naturally explains its insensitivity to the occurrence of a CDW.

Single crystals of $2H$-$NbSe_2$ were grown using the vapor growth technique in sealed quartz tubes with iodine as a transport agent [3]. Typical dimensions of the crystals are $100 \times 100 \times 50\ \mu m^3$ ($\vec{a} \times \vec{b} \times \vec{c}$). Pressure was generated using a diamond anvil cell, loaded with helium as a pressure transmitting medium to ensure highly hydrostatic conditions. Temperature was lowered using a custom-designed ^{4}He cryostat, and pressure was varied *in situ* at low temperature using a helium-pressurized membrane. Each cell contained two rubies to monitor the pressure *in situ* using the fluorescence technique. Measurements of the phonon dispersion of $2H$-$NbSe_2$ were taken between room temperature and 20 K, and for pressures ranging from 0.2 to 16 GPa.

IXS measurements were carried out on beamline ID28 at the European Synchrotron Radiation Facility. The x-ray beam was aligned along the c axis of the crystal. We used the (9,9,9) reflection on the backscattering monochromator with an incident energy of 17.794 keV, and a corresponding energy resolution of 1.3 meV HWHM (Lorentzian fit of the elastic peak). The incident beam was focused by a multilayer mirror into a spot of $100 \times 60\ \mu m$ (width $\times$ height). We used 20×60 mm (width $\times$ height) slits at a 7 m distance giving a momentum resolution of 0.014 $Å^{-1}$ ($a^* \times c^* \approx 2.1 \times 0.50\ Å^{-1}$) in the $(H,0,L)$ plane, and 0.042 $Å^{-1}$[$b^* \times \sin(60^\circ) \approx 1.8\ Å^{-1}$] in the perpendicular direction. We measured the phonon dispersion along the ΓM direction close to Γ_{200} [i.e., $(2-h,0,0)$], where both longitudinal optical and acousticlike soft phonon branches can be observed. According to the balance of the dynamical structure factor of the two phonon modes and so of the inelastic scattering function $S(\mathbf{q},\omega)$, the observation of one of the two branches can be selected. For each transfer wave vector investigated, an energy scan up to 15 meV was performed.

All the spectra were fitted using the standard Levenberg-Marquardt algorithm, with the following free parameters: position and amplitude of the elastic peak; position, linewidth, and amplitude of the phonon; and a constant background. We make the standard assumptions [32,33] that the elastic peak is Lorentzian, and that the phonon line shape can be modeled by a damped harmonic oscillator convoluted by a normalized Lorentzian with a width corresponding to the resolution of the detector.

Ab initio calculations were performed within density functional perturbation theory and the generalized gradient approximation [34] making use of the QUANTUM ESPRESSO [22] code. An ultrasoft pseudopotential (norm conserving) for Nb (Se), a 35 Ry energy cutoff, and a $24 \times 24 \times 8$ mesh for the electronic integrations were used. A Hermitian-Gaussian smearing of 0.01 Ry was used. Harmonic dynamical matrices were calculated within linear response in a grid of $6 \times 6 \times 4$ $\mathbf{q}$ points. The small smearing parameter and the dense electronic mesh used are needed to converge the phonon frequency of the longitudinal acoustic mode at the CDW wave vector (cf. SM). The stochastic self-consistent harmonic approximation (SSCHA) [28,35] calculations were performed using a

$3 \times 3 \times 1$ supercell, yielding anharmonic dynamical matrices in the commensurate $3 \times 3 \times 1$ grid. The difference between the SSCHA dynamical matrices and the harmonic dynamical matrices in the $3 \times 3 \times 1$ grid was Fourier interpolated to the points of the finer $6 \times 6 \times 4$ grid. Adding the harmonic dynamical matrices in the $6 \times 6 \times 4$ grid to the result of the interpolation, the SSCHA dynamical matrices in the finer $6 \times 6 \times 4$ mesh were obtained. The experimental lattice parameters [18] with relaxed internal coordinates were used because in these conditions the results weakly depend on the exchange-correlation potential chosen.

The electron-phonon calculations were performed by using maximally localized Wannier functions [36,37] and interpolation of the electron-phonon matrix elements as in Ref. [38]. We used 14 Wannier functions (d states of Nb and Se p_z states) and a $6 \times 6 \times 4$ electron-momentum grid. We used the Fourier interpolated SSCHA dynamical matrices in the electron-phonon coupling calculations. The average electron-phonon coupling was interpolated using electron and phonon momentum grids of $24 \times 24 \times 8$ randomly displaced from the origin.

The temperature dependence of the low-energy phonon dispersions recorded at pressures of 3.5 and 16 GPa are shown in Fig. 2 (some of the corresponding raw data is shown in the Supplemental Material). At $T = 20$ K and $P = 3.5$ GPa, the system is very close to the quantum critical regime reported in Ref. [18]. No particular enhancement of the elastic line intensity close to the CDW wave vector $\mathbf{q}_{\mathrm{CDW}} \approx (1.67,0,0)$ is observed. On the other hand, a colossal temperature dependent softening of the longitudinal acoustic phonon mode is seen: from $\sim$9 to $\sim$1.5 meV between room temperature and 20 K. While this mode is expected to condense around $\sim$12 K [18], this temperature could not be reached at this pressure with the current experimental setup. As we increase pressure to 16 GPa, the amplitude of the phonon softening is significantly reduced, but remains sizable as the mode's energy almost decreases by a factor of 2 from 300 to 20 K. So far, most of the theoretical and experimental work on $NbSe_2$ has focused on the interplay between the electronic susceptibility and the electron-phonon interaction as possible mechanisms for the CDW formation [39,40]. The large temperature dependence indicates that strong anharmonic effects survive over a pressure range that is way larger than the experimentally reported CDW stability range ($0 < P < P_{CDW}$) and might therefore play an important role that was up to now largely disregarded.

In Fig. 3, we plot the square of the soft phonon frequency measured at $T = 20$ K at $\mathbf{q}_{\mathrm{CDW}}$ as a function of pressure. The linear dependence indicates that the mode hardens as $\sqrt{P - P_{CDW}}$. We also plot the square of the phonon frequency calculated within the harmonic approximation, which is negative—i.e., indicating that the system is unstable against CDW formation—up to 14 GPa $\gg P_{CDW}$. This is reminiscent of the situation encountered at ambient pressure in NbS_2, where we have observed a large phonon softening upon cooling, insufficient, however, to induce the CDW formation despite the predictions of the harmonic *ab initio* calculation [23].

To quantify the effect of anharmonicity and check whether it is responsible for the destabilization of the CDW between P_{CDW} and 14 GPa, we have carried out a series of calculations

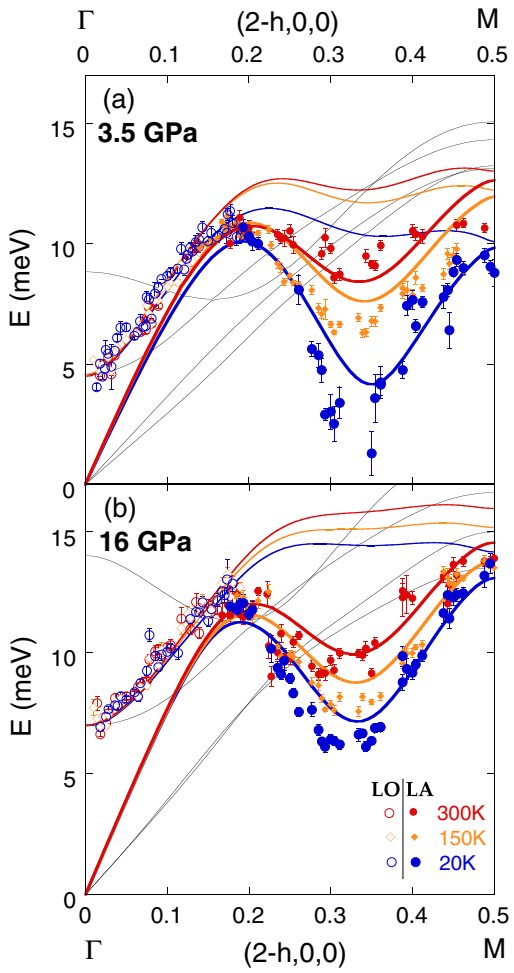

FIG. 2. (Color online) Phonon dispersion at 3.5 GPa (a) and 16 GPa (b). Closed (respectively, open) dots represent the experimentally determined longitudinal acoustic (longitudinal optic) soft phonon dispersions, and lines represent the results of phonon calculations. Close to the Γ point, the phonon dispersion clearly shows an optical branch. Closer to the M point, the energy of the phonon observed corresponds to the acousticlike branch calculated. Colored thick and thin lines represent the SSCHA results for the longitudinal acoustic and optical anharmonic phonons, respectively, at several temperatures. The thin black lines represent other phonon modes present in this energy range calculated within the SSCHA at 20 K, which are very harmonic and barely depend on temperature (see SM).

for the pressures and temperatures experimentally investigated, within the SSCHA approach [28,35] (see SM) which allows us to directly access the anharmonic free energy of the system, with full inclusion of the anharmonic potential terms.

The results are superimposed to our experimental dispersions in Fig. 2. Not only is the instability suppressed as experimentally observed, but the agreement between the measured and calculated dispersions over the entire pressure range is remarkable compared to harmonic *ab initio* calculation. A small overestimation of phonon calculation is nevertheless observed in the range around $\mathbf{q}_{\mathrm{CDW}}$.

A key result here is that, even at low temperature, anharmonic terms play a key role in the destruction of the

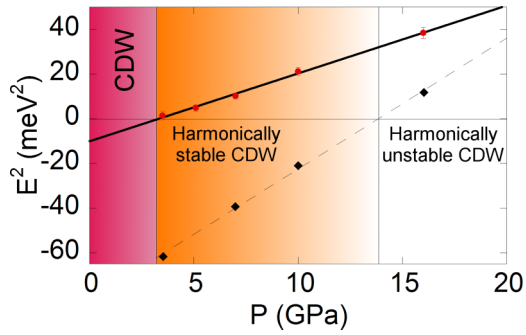

FIG. 3. (Color online) Pressure dependence of the square of the measured energy of the longitudinal acoustic soft phonon at the CDW ordering wave vector and at 20 K (red dots) compared to the square of the energy calculated in the harmonic approximation (black diamonds). Lines are linear fits. The red region indicates the range of pressure where a CDW is observed experimentally at 20 K. The orange region indicates the range of pressure where harmonic calculations predict a CDW ground state.

harmonically stable long-range CDW order. This is surprising at first glance since anharmonic effects usually manifest themselves at finite temperature, through the effect of many-body interactions between thermally excited phonons. These account for the lattice thermal expansion and for the decay of the phonons lifetime at high temperatures, but are usually strongly suppressed at low temperatures. On the other hand, given that atoms vibrate even at zero temperature due to the zero-point fluctuations, their motion can in principle be affected by the anharmonic potential. This appears to be the case in this system where, below 14 GPa, the harmonic part of the potential that drives the lattice instability is overwhelmed by the anharmonic part. The balance between these two parts of the potential tells whether there is a lattice instability (driven by the CDW) or not. This bears stark analogy with the destruction of long-range magnetic order from spin-spin quantum fluctuations in low dimensional quantum magnets [41].

Finally we note that these many-body effects are relevant not only at $\mathbf{q} = \mathbf{q}_{\mathrm{CDW}}$, but extend up to the M point, the boundary of the Brillouin zone at $\mathbf{q} = \mathbf{a}^*/2$, where two low-energy modes, the longitudinal acoustic mode that drives the CDW transition and an optical mode, are substantially hardened with respect to the result of the harmonic calculation.

The importance of the electron-phonon interaction in the CDW formation has been emphasized [12,39], but its role in superconductivity remains debated, as is, more generally, the interplay between these two orders. Indeed, the absence of reliable *ab initio* phonon calculations in the high symmetry phase, has prevented a calculation of the superconducting critical temperature. Having achieved a detailed understanding of the low-energy part of the experimental phonon spectra and having shown how anharmonicity can suppress the long-range-ordered CDW phase, we can now address the superconducting properties of $NbSe_2$ by calculating the Eliashberg function and the integrated electron-phonon coupling (see SM) as a function of pressure. As of now, this calculation can only be done in the high pressure phase, where the number of atoms per unit cell

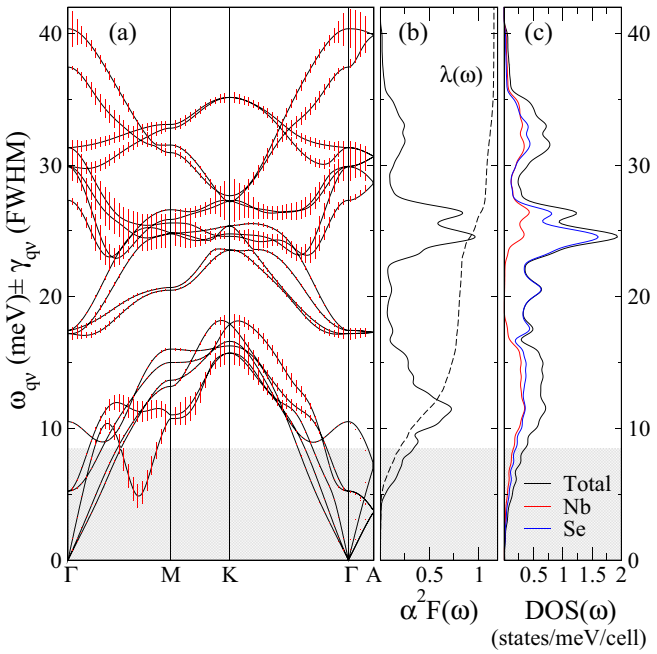

FIG. 4. (Color online) (a) Calculated phonon dispersion at 7 GPa and 0 K with the SSCHA. The size of the bars is proportional to the electron-phonon contribution to the phonon linewidth (the bar is twice the FWHM). (b) The Eliashberg function $\alpha^2F(\omega)$ and the integrated electron-phonon coupling $\lambda(\omega)$. (c) The phonon density of states decomposed into the different atoms. In all figures the gray background denotes the integration area used to infer that the soft acoustic longitudinal mode contributes 17% of the total electron-phonon coupling.

is low enough. We show in Fig. 4 the results of the calculation at 7 GPa (data for other pressures are shown in the SM). We find that the average electron-phonon coupling is as large as $\lambda = 1.16$ (see Table I for other pressures), demonstrating that $NbSe_2$ is a strong coupling superconductor.

Previous works [11,12,16,17,42] identified the large electron-phonon coupling of the soft acoustic mode at $\mathbf{q}_{\mathrm{CDW}}$ as the mechanism responsible for the CDW formation. For this reason, it is natural to expect that this soft mode also plays a key role in superconductivity. However, its contribution to the average electron-phonon coupling is less than 17% [as can be inferred from the integrated $\lambda(\omega)$ in Fig. 4], meaning that it has only a marginal role in superconductivity. Indeed, the strong coupling of this mode is very localized around $\mathbf{q}_{\mathrm{CDW}}$, and its contribution to λ averages out when integrating over the Brillouin zone. The modes sustaining superconductivity are given by the two main contributions to the Eliashberg function:

TABLE I. Calculated λ, logarithmic frequency average $\omega_{\log}$, and T_c values for 2*H*-$NbSe_2$ at 3.5, 7, and 16 GPa. The McMillan equation with $\mu^* = 0.16$ is used to calculate T_c. Experimental data are taken from Ref. [20].

P (GPa)	λ	$\omega_{\log}$ (meV)	T_c calc. (K)	T_c expt. (K)
3.5	1.28	12.6	11.3	7.8
7	1.16	13.7	10.5	8.2
16	0.91	16.4	7.8	7.8

a broad peak centered around ≈11.5 meV and a second one in the 22–26 meV region. These two features contribute to ≈70% of the total electron-phonon coupling. Further insights are obtained by decomposing the phonon density of states (DOS) in atomic vibrations along different directions. As the DOS and $\alpha^2F(\omega)$ are very similar, the decomposition will also apply to the Eliashberg function. The low-energy feature at 11.5 meV is mainly due to Nb and Se vibrations parallel to the Nb plane, corresponding to the flat phonon band along ΓM suffering from a large anharmonic correction, while the features in the 22–26 meV range are mostly attributed to out-of-plane and in-plane Se displacements with a non-negligible Nb component. In both modes sustaining superconductivity there is a substantial Se component, upturning the conventional wisdom that in superconducting dichalcogenides the chalcogene is accessory while the transition metal plays a key role [4]. Our work demonstrates that the superconducting properties strongly depend on both the transition metal and the chalcogene, offering a natural explanation for the different relation between CDW and superconductivity encountered in different dichalcogenides [43–45]. Moreover, as optical phonon modes contribute strongly to superconductivity in $2H$-$NbSe_2$, while the CDW is determined by the softening of the longitudinal acoustic mode, the superconducting T_c is insensitive to the presence of the CDW, explaining the phase diagram in Fig. 1.

Our work points toward the key role of anharmonicity in destroying the CDW order not only through the usual thermal phonon fluctuations, but also through quantum phonon fluctuations, and on a very wide pressure range above the quantum phase transition. Our results, in this respect, are fundamental and relevant for a very large set of materials exhibiting a CDW instability—or more generally a second order electronic quantum phase transition coupled to the lattice—such as transition-metal dichalcogenides, cuprates, Bechgaard salts, and transition metal bronzes.

Sabrina Salmon-Bourmand is thanked for her help in the synthesis of $2H$-$NbSe_2$ single crystals. P.R. and M.L. acknowledge financial support from the French National Research Agency through Grant No. ANR-12-JS04-0003-01 SUBRISSYME. M.C., F.M., and I.E. acknowledge support from the Basque Government (Grant No. BFI-2011-65), Spanish Ministry of Economy and Competitiveness (FIS2013-48286-C2-2-P), Graphene Flagship and ANR (Contract No. ANR-13-IS10-0003-01), and Prace (2014102310). Calculations were performed at IDRIS, CINES, DIPC, and at CEA TGCC.

[1] G. Ghiringhelli *et al.*, Long-range incommensurate charge fluctuations in (Y, Nd)$Ba_2Cu_3O_{6+x}$, Science **337**, 821 (2012).

[2] M. Le Tacon *et al.*, Inelastic x-ray scattering in $YBa_2Cu_3O_{6.6}$ reveals giant phonon anomalies and elastic central peak due to charge-density-wave formation, Nat. Phys. **10**, 52 (2014).

[3] D. E. Moncton, J. D. Axe, and F. J. Di Salvo, Neutron scattering study of the charge-density wave transitions in $2H$-$NbSe_2$ and $2H$-$TaSe_2$ by neutron scattering, Phys. Rev. B **16**, 801 (1977).

[4] J. A. Wilson, F. J. Di Salvo, and S. Mahajan, Charge-density waves and superlattices in the metallic layered transition metal dichalcogenides, Adv. Phys. **24**, 117 (1975).

[5] T. Yokoya, T. Kiss, A. Chainani, S. Shin, M. Nohara, and H. Takagi, Fermi surface sheet-dependent superconductivity in $2H$-$NbSe_2$, Science **294**, 2518 (2001).

[6] T. Valla, A. V. Fedorov, P. D. Johnson, P.-A. Glans, C. McGuinness, K. E. Smith, E. Y. Andrei, and H. Berger, Quasiparticle Spectra, Charge-Density Waves, Superconductivity, and Electron-Phonon Coupling in $2H$-$NbSe_2$, Phys. Rev. Lett. **92**, 086401 (2004).

[7] T. Kiss, T. Yokoya, A. Chainani, S. Shin, T. Hanaguri, M. Nohara, and H. Takagi, Charge-order-maximized momentum-dependent superconductivity, Nat. Phys. **3**, 720 (2007).

[8] I. Guillamon, H. Suderow, F. Guinea, and S. Vieira, Intrinsic atomic-scale modulations of the superconducting gap of $2H$-$NbSe_2$, Phys. Rev. B **77**, 134505 (2008).

[9] S. V. Borisenko, A. A. Kordyuk, V. B. Zabolotnyy, D. S. Inosov, D. Evtushinsky, B. Büchner, A. N. Yaresko, A. Varykhalov, R. Follath, W. Eberhardt, L. Patthey, and H. Berger, Two Energy Gaps and Fermi-Surface "Arcs" in $NbSe_2$, Phys. Rev. Lett. **102**, 166402 (2009).

[10] D. J. Rahn, S. Hellmann, M. Kallne, C. Sohrt, T. K. Kim, L. Kipp, and K. Rossnagel, Gaps and kinks in the electronic structure of the superconductor $2H$-$NbSe_2$ from angle-resolved photoemission at 1 K, Phys. Rev. B **85**, 224532 (2012).

[11] C. J. Arguello *et al.*, Quasiparticle Interference Quasiparticle Interactions and the Origin of the Charge Density Wave in $2H$-$NbSe_2$, Phys. Rev. Lett. **114**, 037001 (2015).

[12] F. Weber, S. Rosenkranz, J. P. Castellan, R. Osborn, R. Hott, R. Heid, K. P. Bohnen, T. Egami, A. H. Said, and D. Reznik, Extended Phonon Collapse and the Origin of the Charge-Density Wave in $2H$-$NbSe_2$, Phys. Rev. Lett. **107**, 107403 (2011).

[13] J. E. Inglesfield, Bonding and phase transitions in transition metal dichalcogenide layer compounds, J. Phys. C **13**, 17 (1980).

[14] C. M. Varma and A. L. Simons, Strong-Coupling Theory of Charge-Density-Wave Transitions, Phys. Rev. Lett. **51**, 138 (1983).

[15] F. Flicker and J. van Wezel, Charge order from orbital-dependent coupling evidenced by $NbSe_2$, Nat. Commun. **6**, 7034 (2015).

[16] M. Calandra, I. I. Mazin, and F. Mauri, Effect of dimensionality on the charge-density wave in few-layer $2H$-$NbSe_2$, Phys. Rev. B **80**, 241108 (2009).

[17] F. Weber, R. Hott, R. Heid, K. P. Bohnen, S. Rosenkranz, J. P. Castellan, R. Osborn, A. H. Said, B. M. Leu, and D. Reznik, Optical phonons and the soft mode in $2H$-$NbSe_2$, Phys. Rev. B **87**, 245111 (2013).

[18] Y. Feng, J. Wang, R. Jaramillo, J. van Wezel, S. Haravifard, G. Srajer, Y. Liue, Z.-A. Xu, P. B. Littlewood, and T. F. Rosenbaum, Order parameter fluctuations at a buried quantum critical point, Proc. Natl. Acad. Sci. USA **109**, 7224 (2012).

[19] C. Berthier, P. Molinié, and D. Jérome, Evidence for a connection between charge density waves and pressure enhancement of superconductivity in $2H$-$NbSe_2$, Solid State Commun. **18**, 1393 (1976).

[20] H. Suderow, V. G. Tissen, J. P. Brison, J. L. Martínez, and S. Vieira, Pressure Induced Effects on the Fermi Surface of Superconducting 2*H*-$NbSe_2$, Phys. Rev. Lett. **95**, 117006 (2005).

[21] See Supplemental Material at http://link.aps.org/supplemental/10.1103/PhysRevB.92.140303 for technical details.

[22] P. Giannozzi *et al.*, QUANTUM ESPRESSO: A modular and open-source software project for quantum simulations of materials, J. Phys. Condens. Matter **21**, 395502 (2009).

[23] M. Leroux, M. Le Tacon, M. Calandra, L. Cario, M. A. Measson, P. Diener, E. Borrissenko, A. Bosak, and P. Rodiere, Anharmonic suppression of charge density waves in 2*H*-NbS_2, Phys. Rev. B **86**, 155125 (2012).

[24] J. D. Budai *et al.*, Metallization of Vanadium dioxide driven by large phonon entropy, Nature (London) **515**, 535 (2014).

[25] O. Delaire *et al.*, Giant anharmonic phonon scattering in PbTe, Nat. Mater. **10**, 614 (2011).

[26] M. Hoesch, P. Piekarz, A. Bosak, M. Le Tacon, M. Krisch, A. Kozlowski, A. M. Oles, and K. Parlinski, Anharmonicity due to Electron-Phonon Coupling in Magnetite, Phys. Rev. Lett. **110**, 207204 (2013).

[27] I. Errea, B. Rousseau, and A. Bergara, Anharmonic Stabilization of the High-Pressure Simple Cubic Phase of Calcium, Phys. Rev. Lett. **106**, 165501 (2011).

[28] I. Errea, M. Calandra, and F. Mauri, First-Principles Theory of Anharmonicity and the Inverse Isotope Effect in Superconducting Palladium-Hydride Compounds, Phys. Rev. Lett. **111**, 177002 (2013).

[29] H. R. Glyde, *Excitations in liquid and solid helium* (Clarendon, Oxford, 1994).

[30] S. E. Rowley, L. J. Spalek, R. P. Smith, M. P. M. Dean, M. Itoh, J. F. Scott, G. G. Lonzarich, and S. S. Saxena, Ferroelectric quantum criticality, Nat. Phys. **10**, 367 (2014).

[31] G. Grüner, *Density waves in solids* (Perseus Books, Cambridge, 2000).

[32] B. Fåk and B. Dorner, Phonon line shapes and excitation energies, Physica B: Condensed Matter **234–236**, 1107 (1997).

[33] E. Burkel, Phonon spectroscopy by inelastic x-ray scattering, Rep. Prog. Phys. **63**, 171 (2000).

[34] J. P. Perdew, K. Burke, and M. Ernzerhof, Generalized Gradient Approximation Made Simple, Phys. Rev. Lett. **77**, 3865 (1996).

[35] I. Errea, M. Calandra, and F. Mauri, Anharmonic free energies and phonon dispersions from the stochastic self-consistent harmonic approximation: Application to platinum and palladium hydrides, Phys. Rev. B **89**, 064302 (2014).

[36] N. Marzari and D. Vanderbilt, Maximally localized generalized Wannier functions for composite energy bands, Phys. Rev. B **56**, 12847 (1997).

[37] I. Souza, N. Marzari, and D. Vanderbilt, Maximally localized Wannier functions for entangled energy bands, Phys. Rev. B **65**, 035109 (2001).

[38] M. Calandra, G. Profeta, and F. Mauri, Adiabatic and nonadiabatic phonon dispersion in a Wannier function approach, Phys. Rev. B **82**, 165111 (2010).

[39] M. D. Johannes, I. I. Mazin, and C. A. Howells, Fermi-surface nesting and the origin of the charge-density wave in $NbSe_2$, Phys. Rev. B **73**, 205102 (2006).

[40] X. Zhu, Y. Caoa, J. Zhang, and E. W. Plummer, Classification of charge density waves based on their nature, Proc. Natl. Acad. Sci. USA **112**, 2367 (2015).

[41] L. Balents, Spin liquids in frustrated magnets, Nature (London) **464**, 199 (2010).

[42] L. P. Gor'kov, Strong electron-lattice coupling as the mechanism behind charge density wave transformations in transition-metal dichalcogenides, Phys. Rev. B **85**, 165142 (2012), and references therein.

[43] V. G. Tissen, M. R. Osorio, J. P. Brison, N. M. Nemes, M. Garcia-Hernandez, L. Cario, P. Rodiere, S. Vieira, and H. Suderow, Pressure dependence of superconducting critical temperature and upper critical field of 2*H*-NbS_2, Phys. Rev. B **87**, 134502 (2013).

[44] A. F. Kusmartseva, B. Sipos, H. Berger, L. Forró, and E. Tutis, Pressure Induced Superconductivity in Pristine 1*T*-$TiSe_2$, Phys. Rev. Lett. **103**, 236401 (2009).

[45] B. Sipos, A. F. Kusmartseva, A. Akrap, H. Berger, L. Forro, and E. Tutis, From Mott state to superconductivity in 1T-TaS_2, Nat. Mater. **7**, 960 (2008).